

Chapter 1

Introduction

1.1 Charge Transport in Organic Semiconductors

1.1.1 Organic Semiconductors

Conductive polymers were first discovered in 1977 by Shirakawa et al^{6,7} for which they were awarded the Nobel prize in Chemistry. Since then, these materials have become widespread in many technologies, such as in organic photovoltaic cells⁸, organic field-effect transistors (OFET)⁹ and organic light-emitting diodes (OLED)¹⁰. While the other two technologies lag behind their inorganic counterparts, uptake of OLED screens is becoming ubiquitous -especially in the smartphone and television market due to their flexibility, better colour representation and lower energy consumption than standard backlit LCD displays. OLEDs have also found uses in lighting with their efficiency rivalling that of fluorescent tubes^{11,12}. Although, industry has made large strides in fabricating and using these materials the exact nature of the charge transport is still poorly understood. Traditional theories (such as hopping and band transport) aren't applicable to many relevant materials^{13–17} as charge transfer dynamics lies in an intermediate region where the charge carrier forms a polaron which is neither fully localised or delocalised. In organic semiconductors, typical values of the localisation of the polaron are between 2 → 20 molecules. This is due to crystals typically being formed of organic molecules weakly held together by Van der Waals (VDW) forces rather than strong covalent bonds. This allows molecules to fluctuate about their lattice sites and introduces larger quantities of (dynamic) disorder than is present in inorganic crystals.

There are a number of techniques currently used in the field to evaluate the performance of organic semiconductors, though all come with their own caveats. For example, transient localisation theory (TLT)^{16,18,19}, while efficient and accurate, cannot be used in non-periodic systems or those with large amounts of static disorder. Another technique, multi-configurational time-dependent Hartree (MCTDH)^{20,21}, is considered the gold standard for wavepacket propagation and has been used extensively in numerous studies (e.g. refs^{22–24}). However, due to the treatment of the full system (including nuclei) quantum mechanically, MCTDH is relatively expensive and can only be applied to a small molecular systems. In this work I will be studying electron-nuclear propagation methods that rely on the treatment of the nuclear degrees of freedom classically and the electronic ones quantum mechanically. This approximation is termed the semi-classical approximation and allows the efficient simulation of mesoscopic systems.

There are a number of semi-classical techniques used in the field. The most common are fewest switches surface hopping (FSSH)²⁵ and mean-field dynamics (also called Ehrenfest dynamics)²⁶. In addition to these, in this work I will be exploring a relative newcomer to the (nonadiabatic) semi-classical simulation arsenal, namely coupled-trajectory mixed quantum-classical molecular dynamics (CTMQC). I will be focussed on the extension of these algorithms and their application to organic semiconducting systems, containing a hundreds of molecules.

1.2 Semi-classical Nonadiabatic Molecular Dynamics

Semi-classical techniques all decompose the nuclear and electronic degrees of freedom and propagate nuclei with Newton's equations using standard molecular dynamics²⁷. Here the forces are calculated with a parameterised forcefield and positions and velocities are often updated with the velocity Verlet technique. The forcefield outlines the shape of the potential energy surface (PES) the nuclei evolve on. The electronic subsystem is propagated using a variety of techniques that solve the time-dependent Schrödinger equation. There are numerous techniques for the calculating electronic properties used in

propagation, though the most common are density functional theory (DFT) and model Hamiltonian based methods. However, in nonadiabatic processes (such as in charge transfer²⁸ or photoexcitation^{29–31}) the nuclear and electronic subsystems are not independent. That is, the specific nuclear geometry depends on the electron density and vice-versa. The resulting interaction between these 2 subsystems is the way each of the semi-classical techniques differ. In this regime the Born-Oppenheimer approximation cannot be applied³². This approximation, relied upon for almost a century³³, hinges on the fact that nuclei are much more massive than electrons and are approximately stationary with respect to electron motion³⁴. This results in nuclear evolution that is governed by a single, adiabatic, potential energy surface. Nonadiabatic molecular dynamics methods, such as the aforementioned surface hopping and mean-field techniques, facilitates the bypassing of this limitation and can be used to simulate molecular dynamics with electronic transitions.

1.2.1 Ehrenfest Dynamics

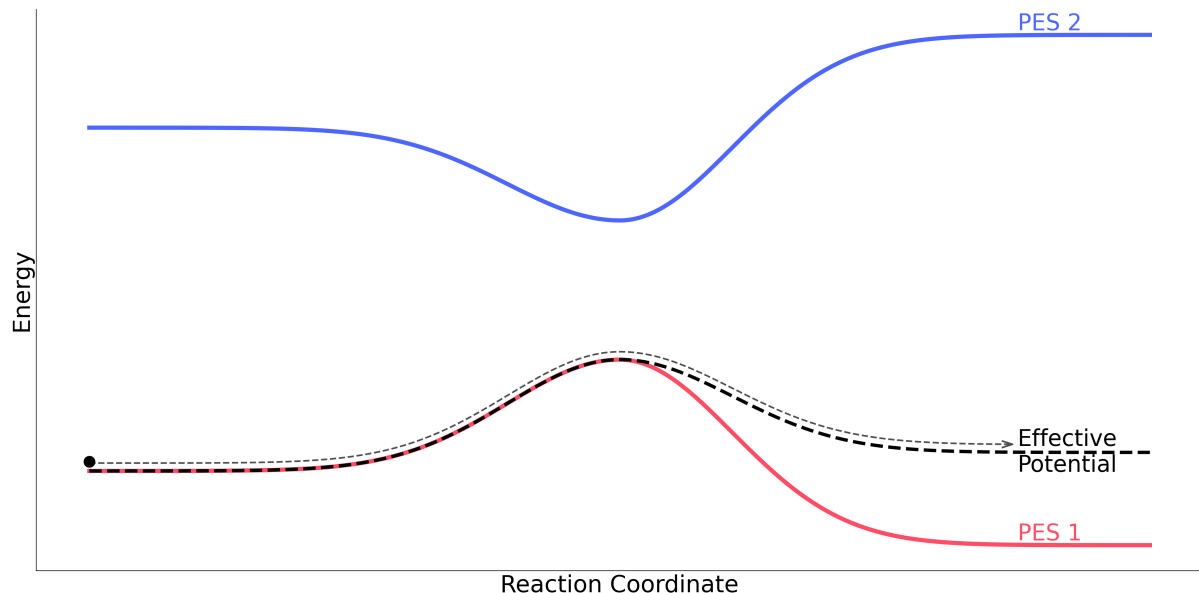


Figure 1.1: An example of a typical Ehrenfest simulation near an avoided crossing. The black lines represent the adiabatic potential energy surface due to the ground (PES 1) and excited (PES 2) state. The red line represents the population weighted average potential the nuclei travel on.

The oldest, and most intuitive, NAMD method is Ehrenfest dynamics⁷. In this technique the nuclei evolve on a single, mean potential energy surface (PES). The shape of this PES comes from a population-weighted average, hence the electronic subsystem can influence the nuclear dynamics through the PES. This is method of propagation is displayed for a simple 1D, 1 atom, 2 state system in figure 1.1. In this figure we initialise the adiabatic population in the ground (red) state. As the atom (black dot) progress through the reaction coordinates it feels forces equal to the negative gradient of the population-weighted average PES (dotted black line).

The Ehrenfest equations can be rigorously derived from the time-dependent Schrödinger equation by expanding the full the full electronic wavefunction as a linear combination of adiabatic states as in equation (1.1) and assuming that the nuclei's motion is determined by a single population-weighted PES. The equation for the calculation of these forces is given in equation (1.2).

$$\Psi(\mathbf{r}, \mathbf{R}, t) = \sum_m C_m(\mathbf{R}, t) \phi_i(\mathbf{r}, t) \quad (1.1)$$

Where the full electronic wavefunction $\Psi(\mathbf{r}, \mathbf{R}, t)$ is expanded as a sum of adiabatic expansion coefficients C_m multiplied by an adiabatic basis function ϕ_i . The norm of the adiabatic expansion coefficients gives the probability of finding the wavefunction in state m .

$$\mathbf{F}_v^{Ehren} = \sum_i^{N_{st}} |C_m|^2 \nabla_v E_m + \sum_{m \neq n}^{N_{st}} C_m^* C_n (E_n - E_m) \mathbf{d}_{ij,v}^{ad} \quad (1.2)$$

Where the force, \mathbf{F} , for each atom, v is the sum of the adiabatic population, $|C_m|^2$, on each state, m , multiplied by the gradient of the adiabatic energy of state $\nabla_v E_m$ plus the sum over pairs of adiabatic states, m and n , of the adiabatic expansion coefficients, $C_{m(n)}$ multiplied by the energy difference $E_n - E_m$ multiplied by the nonadiabatic coupling vector $\mathbf{d}_{ij,v}$ on atom v . The adiabatic energies are calculated as the eigenvalues of the hamiltonian.

The equation for the propagation of the adiabatic expansion coefficients is given in

equation (1.3).

$$i\hbar\dot{C}_m = C_m E_m - i\hbar \sum_n^{N_{st}} C_n \mathbf{d}_{mn}^{ad} \quad (1.3)$$

We can see in this equation any mixing of electronic population between states is initially stimulated by the nonadiabatic coupling elements, d_{nm}^{ad} . This is proportional to the nonadiabatic coupling vector and gives the strength of coupling between the adiabatic states. In figure 1.1 the coupling would be highest near the middle of the figure, where the 2 PES come the closest to each other.

Although the Ehrenfest method has been applied with success in many systems^{35–37} it has a number of key shortcomings. Namely, its inability to capture the branching of the nuclear wavefunction (as propagation occurs on only a single PES) and its poor account of the decoherence of the electronic and nuclear subsystem after an avoided crossing. Ehrenfest also violates detailed balance and prevents the thermodynamic equilibration of the system by populating all adiabatic states evenly^{32,38}. In the limit of infinite states this results in infinite electronic temperature³⁹. For this reason many people choose to use fewest switches surface hopping.

1.2.2 Surface hopping

In surface hopping molecular dynamics

1.2.3 Surface Hopping and Ehrenfest Dynamics

An important technique in the field of mixed quantum classical nonadiabatic molecular dynamics is Ehrenfest dynamics. Assuming we treat the nuclei classically the Ehrenfest equations can be rigorously derived from the electronic Schrödinger equation. This is done by assuming that the nuclei's motion is provided by a single population weighted average potential energy surface. This average is taken from the adiabatic potential energy surfaces (eigenvalues of the Hamiltonian) where weights are provided by the populations of each adiabatic state. This effective potential energy surface is shown in fig 1.1. In this way the electronic subsystem influences the propagation of the nuclei. The propagation of the forces and the electrons are controlled by equations (1.2) and (1.3).

In the above equations C_i is the adiabatic expansion coefficient for state i , E_m is the energy of adiabatic state m , $\mathbf{d}_{mn,v}^{ad}$ is the nonadiabatic coupling (in the adiabatic basis) between states m and n for atom v . The d_{mn}^{ad} are the nonadiabatic coupling elements expressed in the adiabatic basis.

Possibly the most popular technique in NAMD is trajectory surface hopping. In trajectory surface hopping the shape of the potential energy surface is determined by a series of discrete stochastic hops between adiabatic potential energy surfaces³⁸. See fig 1.2. The probability of these hops is determined by the non-adiabatic coupling between states. A swarm of trajectories are used and the probability a hop (non-adiabatic coupling) determines how many of these change state. The nuclear dynamics are dictated by the shape of the energy surface they are travelling on. This method can capture the branching of nuclear wavepacket unlike Ehrenfest. However, it still suffers from a number of issues. The original 'fewest switches' surface

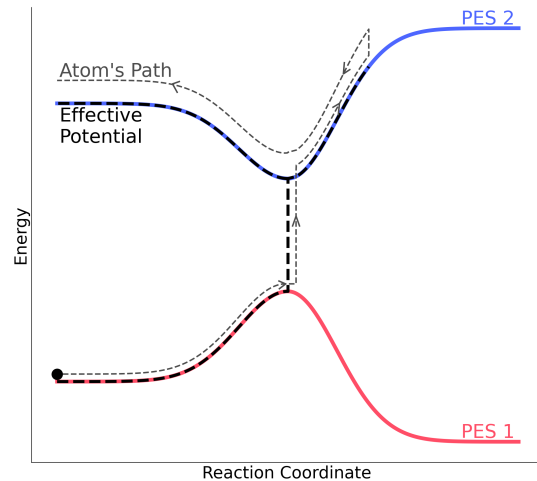


Figure 1.2: An example of a typical Surface Hopping simulation near an avoided crossing. The black lines represent the adiabatic potential energy surface due to the ground (PES 1) and excited (PES 2) state. The red line represents the discontinuous effective potential the nuclei travel on.

hopping' proposed by John Tully suffered from bad overcoherence of the nuclear and electronic subsystems. That is the electronic and nuclear motion was coupled long after the region of high non-adiabatic coupling (crossing region). The fact that the hops are instant leads to discontinuities and methods need to be implemented to fix these such as velocity re-scaling. Finally, perhaps the most important shortcoming is that this technique has not been derived from first principles and cannot be guaranteed to work generally. These problems have lead to a number of other techniques being developed. One of these, CTMQC, will be studied in this thesis and is the semi-classical limit of the exact factorisation of the time-dependent Schrödinger equation.

1.3 Exact Factorisation

Exact factorisation⁴⁰ involves separating the total molecular wavefunction into a nuclear component and electronic component. Where the electronic component is parametrically dependent on the nuclear coordinates, \mathbf{R} . This is shown below in eq (1.4) where χ is the nuclear wavefunction and Φ is the electronic one.

$$\Psi(\mathbf{R}, \mathbf{r}, t) = \Phi_{\mathbf{R}}(\mathbf{r}, t)\chi(\mathbf{R}, t) \quad (1.4)$$

In the above equation (and throughout this report) I will denote nuclear coordinates and electronic coordinates R and r respectively. The nuclear and electronic wavefunctions then obey separate, but coupled, time-dependent Schrödinger equations for spatial and temporal evolution. In this report, I will be focussing on the semi-classical limit of these equations, named Coupled-Trajectory Mixed Quantum-Classical Molecular Dynamics (CTMQC), and give results of a combination of this and the AOM method explained in section ??.

The equations for the evolution of the electronic and nuclear wavefunctions in the exact factorisation⁴⁰ are given below:

$$\hbar \frac{\delta}{\delta t} \Phi_{\mathbf{R}}(\mathbf{r}, t) = (\hat{H}_{BO} + \hat{U}_{en}[\Phi_{\mathbf{R}}, \chi] - \varepsilon(\mathbf{R}, t)) \Phi_{\mathbf{R}}(\mathbf{r}, t) \quad (1.5)$$

$$\hbar \frac{\delta}{\delta t} \chi(\mathbf{R}, t) = \left(\sum_{v=1}^{N_n} \frac{[-\hbar \nabla_v + \mathbf{A}_v(\mathbf{R}, t)]^2}{2M_v} + \varepsilon(\mathbf{R}, t) \right) \chi(\mathbf{R}, t) \quad (1.6)$$

Where \hat{H}_{BO} is the Born-Oppenheimer Hamiltonian, that is $\hat{T}_e + \hat{W}_{ee} + \hat{W}_{nn} + \hat{V}_{en}$. Where \hat{T}_e is the electronic kinetic energy operator, $\hat{W}_{ee/nn}$ is the electron-electron/nuclei-nuclei interaction and V_{en} is the electronic-nuclear potential.

The \hat{U}_{en} is an electronic-nuclear coupling operator (ENCO). This is defined as

$$\hat{U}_{en}[\Phi_{\mathbf{R}}, \chi] = \sum_{v=1}^{N_{nuc}} \frac{1}{M_v} \left[\frac{[-\hbar \nabla_v - \mathbf{A}_v(\mathbf{R}, t)]^2}{2} + \left(\frac{-\hbar \nabla_v \chi}{\chi} + \mathbf{A}_v(\mathbf{R}, t) \right) \left(-\hbar \nabla_v - \mathbf{A}_v(\mathbf{R}, t) \right) \right] \quad (1.7)$$

Where the \mathbf{A}_v is a time-dependent vector potential (TDVP), given by $\langle \Phi_{\mathbf{R}}(t) | -\hbar \nabla_v \Phi_{\mathbf{R}} \rangle_{\mathbf{r}}$ and M_v is the mass of nuclei v . Finally $\epsilon(\mathbf{R}, t)$ is a time-dependent scalar potential energy surface (TDPES), given by $\langle \Phi_{\mathbf{R}}(t) | \hat{H}_{BO} + \hat{U}_{en}^{coup} - \hbar \frac{\delta}{\delta t} | \Phi_{\mathbf{R}}(t) \rangle_{\mathbf{r}}$.

The effects of the TDPES, TDVP and the ENCO have been investigated in multiple works^{1,41–44}. The TDPES and TDVP are both responsible for the evolution of the system⁴¹. The TDPES provides exact classical forces on the nuclei. In fact, an alternative independent-trajectory semi-classical scheme has been investigated using these exact forces¹. This found the TDPES is responsible for the splitting of the nuclear wavepacket in regions of high non-adiabaticity by taking the shape of a step function between the 2 adiabatic potentials. This is demonstrated in figure 1.3, which was adapted from an image in Agostini, 15⁴¹.

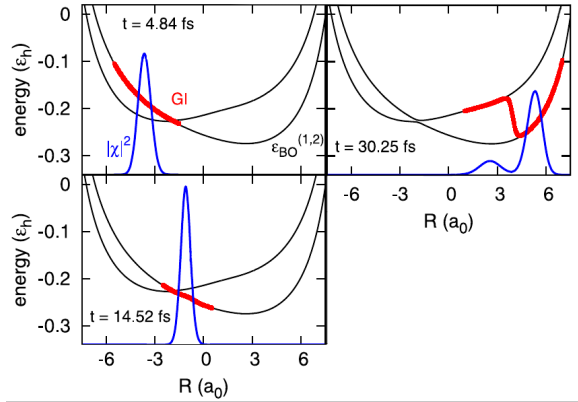


Figure 1.3: A demonstration of how the TDPES can cause the splitting of the nuclear wavepacket in non-adiabatic regions. The red line represents the TDPES and the blue is the nuclear density. Figure adapted from Agostini, 15¹

Finally the electronic-nuclear coupling operator (ENCO) is responsible for other non-adiabatic effects in the system such as electronic nonadiabatic transitions and decoherence⁴¹.

1.4 Approximations leading to CTMQC

Starting from the exact factorisation equations, 6 approximations have been made to derive the CTMQC equations. These are discussed in detail in Ref. 2. In the interest of completeness I have summarised them below.

1.4.1 Classical Nuclei

Techniques that include nuclear quantum effects (NQEs); such as multiple spawning⁴⁵, ring-polymer surface hopping⁴⁶ and nonadiabatic Bohmian dynamics^{47,48} although extremely accurate, cannot be applied to hundreds or thousands of molecules, due to their high computational cost. Further, in many systems of interest NQEs are negligible, especially at room temperature. For this reason the classical limit of the nuclear Schrödinger equation (1.6) is taken when deriving the CTMQC equations.

1.4.2 Neglect the ENCO in the TDPES

The electron-nuclei coupling operator is omitted in the expression for the time-dependent potential energy surface. This is justified as the first term ($(-\hbar\nabla_{\mathbf{v}} - \mathbf{A}_{\mathbf{v}}(\mathbf{R}, t))^2$) contains a second order derivative which is expensive to calculate and has a negligible effect compared to the second term in the ENCO⁴⁹. However, the rest of the ENCO is equal to zero when averaged over $\Phi_{\mathbf{R}}(\mathbf{r}, t)$ so it does not contribute to the TDPES.

1.4.3 Derivative of the Adiabatic Coefficients

The derivative of the adiabatic coefficients appears in the electronic evolution equations. However, we can re-write the derivative of the adiabatic coefficients in terms of their modulus and phase:

$$\nabla_{\mathbf{v}} C_l^{(I)}(t) = \left[\underbrace{\frac{\nabla_{\mathbf{v}} |C_l^{(I)}(t)|}{|C_l^{(I)}(t)|}}_{\text{(Term 1)}} + \underbrace{\frac{i}{\hbar} \nabla_{\mathbf{v}} \gamma_l^{(I)}(t)}_{\text{(Term 2)}} \right] C_l^{(I)}(t) \quad (1.8)$$

It has been found that the first term is negligible compared to the second^{1,42,43} so it doesn't need to be calculated and we can remove it. It was also assumed that the NACVs are localised in space meaning that, after some algebra, the spatial derivative of the adiabatic coefficient can be written as:

$$\nabla_{\mathbf{v}} C_l^{(I)}(t) = \frac{i}{\hbar} \nabla_{\mathbf{v}} \gamma_l^{(I)}(t) C_l^{(I)}(t) = -\frac{i}{\hbar} \int^t dt' \nabla_{\mathbf{v}} \epsilon_l^{(I)} C_l^{(I)}(t') = -\frac{i}{\hbar} \mathbf{f}_l^{(I)} C_l^{(I)}(t) \quad (1.9)$$

Where $\epsilon_l^{(I)}$ is the energy of the l^{th} adiabatic potential energy surface for trajectory I, $C_l^{(I)}$ is the adiabatic expansion coefficient for state l and trajectory I. The $\mathbf{f}_l^{(I)}$ is the time-integrated adiabatic force (adiabatic momentum).

1.4.4 Gaussian Nuclear Wavepackets

In order to calculate the quantum momentum -the new term in CTMQC. Knowledge of the nuclear distribution is needed. However, as we treat the nuclei as point particles we need to re-construct the nuclear density from the atomic positions. This is done by smoothing out the atomic positions by placing a gaussian of width σ centered on each atomic position and combining these gaussians to produce the final nuclear density. This introduces an empirical parameter (σ) which will be discussed later in this thesis. It should be noted, the nuclei are still propagated classically, the width parameter is only used in the calculation of the quantum momentum.

1.4.5 Separating the Effects of Decoherence and NACVs

So as to not introduce any population transfer (due to the quantum momentum) when the NACV is zero a fifth approximation has been introduced. Namely the quantum momentum depends on pairs of states -l,k. This enables the separation of the ‘competing’ effects of the NACV and the Quantum Momentum.

1.5 The CTMQC equations

1.5.1 Adiabatic Basis

The equations for the propagation of the classical nuclei and the expansion coefficients in the CTMQC framework in the adiabatic basis are given below:

$$\dot{\mathbf{P}}_v^{(I)} = \underbrace{-\sum_k |C_k^{(I)}|^2 \nabla_v \epsilon_k^{(I)} - \sum_{k,l} C_l^{(I)} C_k^{*(I)} (\epsilon_k^{(I)} - \epsilon_l^{(I)})}_{\text{Ehrenfest}} - \underbrace{\sum_{l,k} |C_l^{(I)}|^2 \left(\sum_{v'=1}^{N_n} \frac{2}{\hbar M_{v'}} \mathcal{Q}_{lk,v'}^{(I)} \cdot \mathbf{f}_{l,v'}^{(I)} \right) \left[|C_k^{(I)}|^2 \mathbf{f}_{k,v}^{(I)} - \mathbf{f}_{l,v}^{(I)} \right]}_{\text{Quantum Momentum}} \quad (1.10)$$

$$\dot{C}_l^{(I)} = \underbrace{-\frac{i}{\hbar} \epsilon_l^{(I)} C_l - \sum_k C_k^{(I)} d_{lk}^{ad(I)}}_{\text{Ehrenfest}} - \underbrace{\sum_{v=1}^{N_n} \sum_k \frac{\mathcal{Q}_{lk,v}^{(I)}}{\hbar M_v} \cdot [\mathbf{f}_{k,v}^{(I)} - \mathbf{f}_{l,v}^{(I)}] |C_k^{(I)}|^2 C_l^{(I)}}_{\text{Quantum Momentum}} \quad (1.11)$$

Where the ϵ_k term is the potential energy on the k^{th} potential energy surface. C_l is the adiabatic expansion coefficient corresponding to the l^{th} state. The sum over k and l indicates a sum over all states, the (I) superscript is a replica index and the v is an atom index. M_v is the nuclear mass and $d_{lk}^{ad(I)}$ represents the non-adiabatic coupling element (in the adiabatic basis) between adiabatic states l and k . The 2 new terms in this scheme not seen in other NAMD methods are the $\mathcal{Q}_{lk,v}^{(I)}$ and the $\mathbf{f}_{k,v}^{(I)}$. These are the quantum momentum and the adiabatic momentum. The adiabatic momentum term is defined in equation (1.9) this keeps a record of the previous forces on each adiabatic state in the system. The quantum momentum term couples the trajectories together (making this a coupled-trajectory scheme). Together the history dependent force and quantum momentum are responsible for the decoherence in the ‘Quantum Momentum’ parts of the above equations³. Notably, although these equations have been derived from the exact factorisation equations separately from Ehrenfest they do contain the Ehrenfest equations within them (marked ‘Ehrenfest’). This scheme can therefore be seen as an Ehrenfest scheme with a correction that captures branching of the nuclear wavefunction and decoherence within it.

We can also see in equation (1.11) if we are in a pure adiabatic state i.e. all population on a single adiabatic state, there is no contribution from the quantum momentum part of the equations. In this scenario the evolution equations become simply Ehrenfest equations. For example, if all the population is localised on a single adiabatic state then the term $|C_k^{(I)}|^2 C_l$ is only non-zero when $l = k$. However, when $l = k$, the term $[\mathbf{f}_{k,v}^{(I)} - \mathbf{f}_{l,v}^{(I)}]$ is zero as $\mathbf{f}_{k,v}^{(I)} = \mathbf{f}_{l,v}^{(I)}$. Therefore, the quantum momentum term can be seen to only kick in when there is a mixing of adiabatic states. In the adiabatic formulation of these equations it is the adiabatic NACV $\mathbf{d}_{lk,v}^{ad,(I)}$ that is responsible for the initial mixing of the

populations from pure adiabatic states.

1.6 Calculating the Quantum Momentum

The technique for calculating the quantum momentum term is outlined in detail in the SI of min, 17⁵⁰. The original equations given in Agostini, 16² present a quantum momentum term without state indices (l,k). This, due to approximations made in the derivation of CTMQC, results in population transfer even when the non-adiabatic couplings between states are zero. Therefore, Agostini et al enforced this condition with the pair-wise state dependence on the quantum momentum. The quantum momentum is defined in equation (1.12) as:

$$\mathcal{Q}_v^{(I)} = \frac{-\hbar \nabla_v |\chi^{(I)}|}{|\chi^{(I)}|} \frac{-\hbar \nabla_v |\chi^{(I)}|^2}{2|\chi^{(I)}|^2} \quad (1.12)$$

In order to reconstruct the nuclear density, Gaussian distributions are used as in equation (1.13) below:

$$|\chi^{(I)}(t)|^2 = \frac{1}{N_{tr}} \sum_{J=1}^{N_{tr}} \prod_{v=1}^{N_n} g_{\sigma_v^{(J)}(t)} \left(\mathbf{R}_v^{(I)}(t) - \mathbf{R}_v^{(J)}(t) \right) \quad (1.13)$$

Where, N_{tr} is the number of trajectories, N_n is the number of atoms, $\sigma_v^{(J)}(t)$ is a time-dependent width parameter for each gaussian g and $\mathbf{R}_v^{(J)}$ represents the atomic position of atom v on trajectory J .

This results in a linear expression for the quantum momentum. The full details of the derivation are given in the supplementary information of Min, 17⁵⁰. The resulting linear expression for the quantum momentum is given below:

$$\mathcal{Q}_{lk,v}^{(I)} = \alpha_v^{(I)} \mathbf{R}_v^{(I)} - \mathbf{R}_{lk,v} \quad (1.14)$$

Where $\mathbf{R}_v^{(I)}$ are the nuclear coordinates on trajectory I on atom v . The $\alpha_v^{(I)}$ term is a weighted average over trajectories of the product of the gaussian's assigned to each atomic

coordinate, i.e:

$$\alpha_v^{(I)} = \sum_J^{N_{tr}} \frac{\hbar \prod_{v'} g_{\sigma_{v'}^{(J)}(t)} \left(\mathbf{R}_{v'}^{(I)}(t) - \mathbf{R}_{v'}^{(J)}(t) \right)}{2\sigma_v^{(J)}(t)^2 \sum_K^{N_{tr}} \prod_{v'} g_{\sigma_{v'}^{(K)}(t)} \left(\mathbf{R}_{v'}^{(I)}(t) - \mathbf{R}_{v'}^{(K)}(t) \right)} \quad (1.15)$$

Along with the $\mathbf{R}_{lk,v}$ term the $\alpha_v^{(I)}$ performs the job of coupling the trajectories together. The $\mathbf{R}_{lk,v}$ term also given in the SI of Min, 17⁵⁰ is defined for each Cartesian dimension as:

$$R_{lk,v} = \sum_I^{N_{tr}} R_v^{(I)}(t) \alpha_v^{(I)}(t) \frac{|C_k^{(I)}(t)|^2 |C_l^{(I)}(t)|^2 (f_{k,v}^{(I)}(t) - f_{l,v}^{(I)}(t))}{\sum_J |C_k^{(J)}(t)|^2 |C_l^{(J)}(t)|^2 (f_{k,v}^{(J)}(t) - f_{l,v}^{(J)}(t))} \quad (1.16)$$

Where the bold notation for vectors has been replaced by normal font. This means that this equation applies to each Cartesian dimension independently. Further, in this expression $R_{lk,v}$ is symmetric, $R_{lk} = R_{kl}$ meaning that $Q_{lk} = Q_{kl}$. It is also undefined on the diagonals as the denominator is 0, diagonal values are therefore set to 0. At first sight, the R_{lk} term seems to be another weighted average. However, this isn't quite the case as the denominator can be negative. This causes equation (1.16) to be very sensitive to errors in the calculation of the denominator of this fraction. Any inaccuracies can lead to the denominator approaching zero faster than the numerator causing large spikes in the quantum momentum term. This will be discussed in greater detail in the following chapters.

Appendix A

Tully Model Paramters

A.1 Model 1 -Single Avoided Crossing

	Quantity	Value	Unit
Hamiltonian Paramters:			
$H_{11}(\mathbf{R}) = A \tanh(B\mathbf{R})$	Initial Position	-20	a.u.
$H_{12}(\mathbf{R}) = Ce^{-D\mathbf{R}^2}$	Initial Velocities	15.0, 25.0	a.u.
$H_{21}(\mathbf{R}) = H_{12}(\mathbf{R})$	Initial Adiab Pop	ground state	-
$H_{22}(\mathbf{R}) = -H_{11}(\mathbf{R})$	Simulation Time	6000, 4000	a.u.
Where $A = 0.03$, $B = 0.4$, $C = 0.005$ and $D = 0.3$	$\sigma_v^{(I)}$	0.5	a.u.
	M (σ constant)	40	-
	$\Delta t_{\text{nuclear}}$	0.1	fs
	$\Delta t_{\text{electronic}}$	0.01	fs
	$\frac{\delta \mathbf{R}_{lk,v}^{(I)}}{\delta t}$ threshold	0.15	a.u.
	N_{rep}	200	-

A.2 Model 2 -Dual Avoided Crossing

	Quantity	Value	Unit
Hamiltonian Paramters:			
$H_{11}(\mathbf{R}) = 0$	Initial Position	-8	a.u.
$H_{12}(\mathbf{R}) = Ce^{-D\mathbf{R}^2}$	Initial Velocities	16.0, 30.0	a.u.
$H_{21}(\mathbf{R}) = H_{12}(\mathbf{R})$	Initial Adiab Pop	ground state	-
$H_{22}(\mathbf{R}) = -Ae^{-B\mathbf{R}^2} + E$	Simulation Time	2500, 1500	a.u.
Where A = 0.1, B = 0.28, C = 0.015, D = 0.06 and E = 0.05	$\sigma_v^{(I)}$	0.5	a.u.
	M (σ constant)	40	-
	$\Delta t_{\text{nuclear}}$	0.1	fs
	$\Delta t_{\text{electronic}}$	0.01	fs
	$\frac{\delta \mathbf{R}_{ik,v}^{(I)}}{\delta t}$ threshold	0.15	a.u.
	N_{rep}	200	-

A.3 Model 3 -Extended Coupling

	Quantity	Value	Unit
Hamiltonian Paramters:			
$H_{11}(\mathbf{R}) = A$	Initial Position	-15	a.u.
$H_{12}(\mathbf{R}) = \begin{cases} Be^{C\mathbf{R}}, & R \leq 0 \\ B(2 - e^{-C\mathbf{R}}), & R > 0 \end{cases}$	Initial Velocities	10, 30	a.u.
$H_{21}(\mathbf{R}) = H_{12}(\mathbf{R})$	Initial Adiab Pop	ground state	-
$H_{22}(\mathbf{R}) = -H_{11}(\mathbf{R})$	Simulation Time	5000, 1500	a.u.
Where A = 6×10^{-4} , B = 0.1 and C = 0.9	$\sigma_v^{(I)}$	0.5	a.u.
	M (σ constant)	40	-
	$\Delta t_{\text{nuclear}}$	0.1	fs
	$\Delta t_{\text{electronic}}$	0.01	fs
	$\frac{\delta \mathbf{R}_{ik,v}^{(I)}}{\delta t}$ threshold	0.15	a.u.
	N_{rep}	200	-

A.4 Model 4 -Dual Arch

Hamiltonian Paramters:

$$H_{11}(\mathbf{R}) = A$$

$$H_{12}(\mathbf{R}) = \begin{cases} B \left[-e^{C(\mathbf{R}-D)} + e^{C(\mathbf{R}+D)} \right] & R \leq -D \\ B \left[e^{-C(\mathbf{R}-D)} - e^{-C(\mathbf{R}+D)} \right] & R \geq D \\ B \left[2 - e^{C(\mathbf{R}-D)} - e^{-C(\mathbf{R}+D)} \right] & -D < R < D \end{cases}$$

$$H_{21}(\mathbf{R}) = H_{12}(\mathbf{R})$$

$$H_{22}(\mathbf{R}) = -H_{11}(\mathbf{R})$$

Where $A = 6 \times 10^{-4}$, $B = 0.1$, $C = 0.9$ and

$$D = 4$$

Quantity	Value	Unit
Initial Position	-20	a.u.
Initial Velocities	10, 40	a.u.
Initial Adiab Pop	ground state	-
Simulation Time	6000, 2000	a.u.
$\sigma_v^{(I)}$	0.5	a.u.
M (σ constant)	40	-
$\Delta t_{\text{nuclear}}$	0.1	fs
$\Delta t_{\text{electonic}}$	0.01	fs
$\frac{\delta \mathbf{R}_{lk,v}^{(I)}}{\delta t}$ threshold	0.15	a.u.
N_{rep}	200	-

Appendix B

Wigner Distribution Derivation

The nuclear wavepacket (at time 0) is given by:

$$\chi(R) = \frac{1}{(\pi\mu^2)^{\frac{1}{4}}} e^{-\frac{(R-R_0)^2}{2\mu^2} + ik_0(R-R_0)} \quad (\text{B.1})$$

The Wigner quasiprobability function for momentum and position (p, R) is given by:

$$W(p, R) = \frac{1}{\pi\hbar} \int_{-\infty}^{\infty} \chi^*(R+y)\chi(R-y)e^{\frac{2ipy}{\hbar}} dy \quad (\text{B.2})$$

However, both Ehrenfest and CTMQC require atomic positions as input so we must extract the position and velocity probability densities from this. We get these from the marginal integrals of the Wigner distribution i.e.

$$|f(R)|^2 = \int_{-\infty}^{\infty} W(R, p) dp \quad (\text{B.3})$$

$$|f(p)|^2 = \int_{-\infty}^{\infty} W(R, p) dR \quad (\text{B.4})$$

In order to calculate these marginal integrals we must first crunch through the maths of equation (B.2). Substituting eq (B.1) into (B.2):

$$W(p, R) = \frac{1}{\pi\hbar} \int_{-\infty}^{\infty} \frac{1}{\mu\sqrt{\pi}} e^{-\frac{(R+y-R_0)^2}{2\mu^2} - 2ik_0y - \frac{(R-y-R_0)^2}{2\mu^2}} e^{\frac{2ipy}{\hbar}} dy \quad (\text{B.5})$$

Simplifying the 2 quadratic equations (equation (B.5)) we get:

$$W(p, R) = \frac{1}{\pi \hbar} \int_{-\infty}^{\infty} \frac{1}{\mu \sqrt{\pi}} e^{-\mu^{-2}(y^2 - 2ik_0 y \mu^2 + (R-R_0)^2)} e^{\frac{2ipy}{\hbar}} dy \quad (\text{B.6})$$

We can now take the expressions not dependant on y outside of the integral and combine the exponents.

$$W(p, R) = \frac{1}{\pi \sqrt{\pi} \mu \hbar} e^{-\frac{(R-R_0)^2}{\mu^2}} \int_{-\infty}^{\infty} e^{-\frac{y^2 + 2iy\mu^2(\frac{p}{\hbar} - k_0)}{\mu^2}} dy \quad (\text{B.7})$$

Integrating we get:

$$\int e^{-\frac{y^2 + 2iy\mu^2(\frac{p}{\hbar} - k_0)}{\mu^2}} dy = \frac{\sqrt{\pi} \mu}{2} e^{-\frac{\mu^2}{\hbar^2}(p - \hbar k_0)^2} \operatorname{erf} \left[\frac{y}{\mu} + i \left(\frac{p\mu}{\hbar} - \mu k_0 \right) \right] \quad (\text{B.8})$$

Applying limits we get:

$$\int_{-\infty}^{\infty} e^{-\frac{y^2 + 2iy\mu^2(\frac{p}{\hbar} - k_0)}{\mu^2}} dy = \sqrt{\pi} \mu e^{-\frac{\mu^2}{\hbar^2}(p - \hbar k_0)^2} \quad (\text{B.9})$$

Substituting this back into the Wigner distribution (equation (B.2)) we finally get:

$$W(p, R) = \frac{1}{\pi \hbar} e^{-\frac{(R-R_0)^2}{\mu^2}} e^{-\frac{(p - \hbar k_0)^2}{\hbar^2/\mu^2}} \quad (\text{B.10})$$

Taking the marginal integrals we get the position and velocity probability distributions:

$$|f(R)|^2 = \frac{2}{\mu \sqrt{\pi}} e^{-\frac{(R-R_0)^2}{\mu^2}} \quad (\text{B.11})$$

$$|f(p)|^2 = \frac{2}{\frac{\hbar}{\mu} \sqrt{\pi}} e^{-\frac{\mu^2}{\hbar^2}(p - \hbar k_0)^2} \quad (\text{B.12})$$

The above distributions are randomly sampled to get initial atomic velocities and positions for each simulation.

Appendix C

$\mathbf{R}_{lk,v}$ Alternatives

C.1 $\mathbf{R}_{lk,v}$ Extrapolation

C.2 Alternative Quantum Momentum Intercept

In Agostini, 16² another quantum momentum intercept term is discussed. This term is not used because, as previously discussed in section 1.4, it leads to unphysical transfer of population between adiabatic states when the nonadiabatic coupling elements are 0. However, it can be used in these Tully Models as an effective fix to the discontinuities caused by the $\mathbf{R}_{lk,v}$ term.

The other quantum momentum intercept, $\mathbf{R}_{0,v}^{(I)}$, comes directly from the construction of the nuclear density using a linear combination of a product of gaussians (see equation (1.13) in the introduction). It is defined as in equation (C.1) below:

$$\mathbf{R}_{0,v}^{(I)} = \sum_{J}^{N_{tr}} \left[\frac{\hbar \prod_{v'} g_{\sigma_{v'}^{(J)}(t)} \left(\mathbf{R}_{v'}^{(I)}(t) - \mathbf{R}_{v'}^{(J)}(t) \right)}{2 \sigma_v^{(J)}(t)^2 \sum_{K}^{N_{tr}} \prod_{v'} g_{\sigma_{v'}^{(K)}(t)} \left(\mathbf{R}_{v'}^{(I)}(t) - \mathbf{R}_{v'}^{(K)}(t) \right)} \mathbf{R}_v^{(I)} \right] \quad (\text{C.1})$$

However, as switching to this intercept directly may cause discontinuities in itself a smoothing parameter is applied to ease the switch. This is given in equation (C.2) below:

$$[1 - A(t)] R_{good}(t) + A(t) R_{bad}(t) = R_{effective}(t) \quad (\text{C.2})$$

R_{good} refers to the intercept that should be switched to (e.g. for the detection of a spike in the $R_{lk,v}^{(I)}$ we switch to the intercept in in equation (C.1)). $R_{lk,v}^{(I)}$ refers to the intercept that is being switched from (e.g. when it is detected that the divergence of $R_{lk,v}^{(I)}$ has finished then we switch from the alternative intercept back to $R_{lk,v}^{(I)}$). $A(t)$ is a smoothing parameter and is given in equation (C.3) below:

$$A(t) = \frac{D_v^{(I)}}{2} \left[\tanh\left(t - \frac{t_{final} + t_{init}}{0.6Ndt}\right) + 1 \right] \quad (\text{C.3})$$

Where $D_v^{(I)}$ is the distance between the 2 intercepts (e.g. $D_v^{(I)} = R_{lk,v}^{(I)} - R_{0,v}^{(I)}$), N is the number of steps to take before settling solely on one intercept, t_{init} is the time of detection of the divergence, t_{final} is the time at which the code settles on 1 intercept and dt is the timestep taken.

A cartoon of this process is given in figure C.1

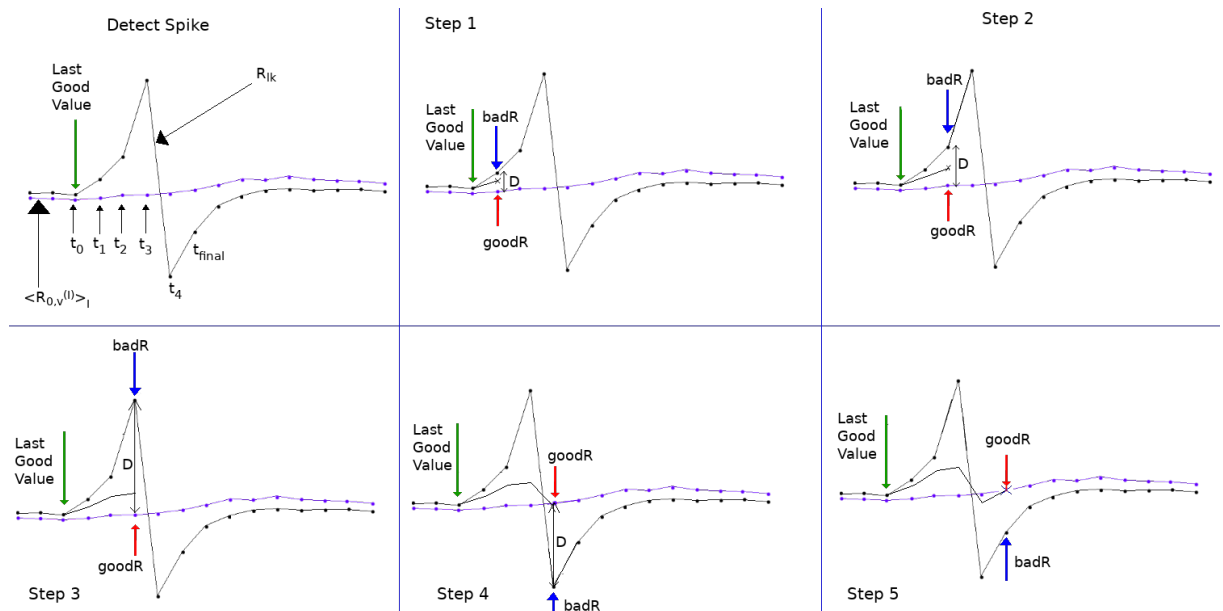


Figure C.1: A crude demonstration of the principle behind the smoothing procedure in switching between intercepts. The black line shows an intercept begin to diverge and the alternative intercept is shown in purple. As the step is incremented the amount of the alternative intercept that makes up the effective intercept is increased until only 1 intercept is used.

Appendix D

Rabi Oscillation

The time dependant Schrödinger equation is given below:

$$\hbar \frac{\delta}{\delta t} \Phi(\mathbf{R}(t), t) = \hat{H}(\mathbf{R}(t), t) \Phi(\mathbf{R}(t), t) \quad (\text{D.1})$$

If we hold the nuclear coordinates in place (e.g. remove time-dependence from nuclear coordinates) we get an ordinary differential equation as shown below:

$$\hbar \frac{d}{dt} \Phi(\mathbf{R}, t) = \hat{H}(\mathbf{R}, t) \Phi(\mathbf{R}, t) \quad (\text{D.2})$$

This has the following general solution. This can be solved with a Taylor series expansion.

$$\Phi(\mathbf{R}, t) = e^{\hbar \hat{H} t} \Phi(\mathbf{R}, 0)$$

Figure

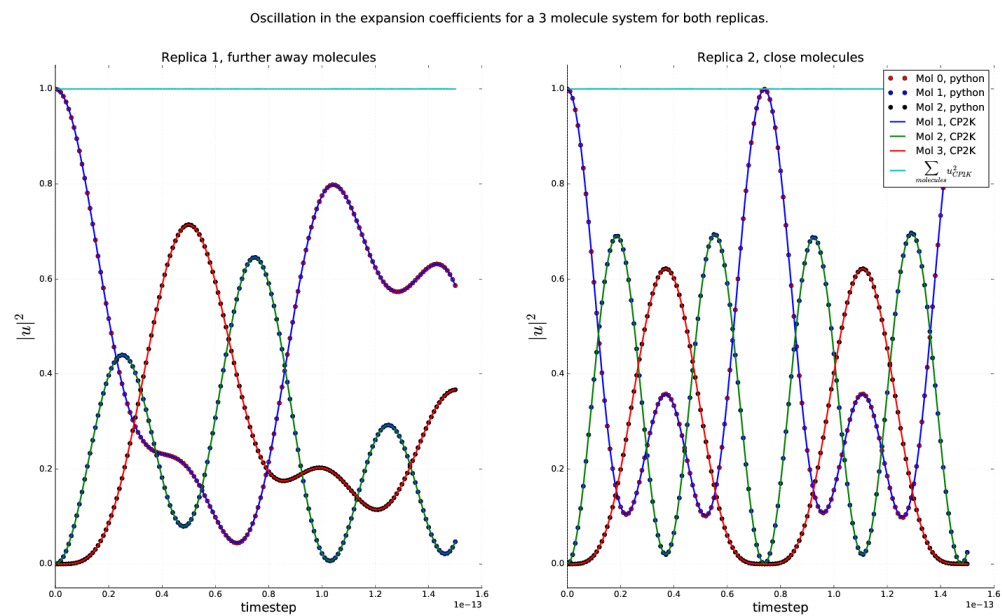


Figure D.1: Rabi oscillation occurring within a Ethylene trimer system. Dotted lines were calculated using equation (D.2), solid lines were calculated using the RK4 propagator within the CTMQC section of the CP2K code. The norm is shown on the top as a cyan line and the x axis shows the timestep in seconds.

Appendix E

Norm Conservation in CTMQC and Ehrenfest

A statement of the conservation of the norm, for a single trajectory, is given below in equation (E.1)

$$\frac{d}{dt} \sum_l |C_l(t)|^2 = \sum_l C_l^*(t) \frac{dC_l(t)}{dt} + \frac{dC_l^*(t)}{dt} C_l(t) = 2\mathbb{R} \left[\sum_l C_l(t)^* \frac{dC_l(t)}{dt} \right] \quad (\text{E.1})$$

Substituting the equation for the evolution of the adiabatic coefficients (and removing the purely imaginary term) into (??) we get equation (E.3)

$$\frac{d}{dt} \sum_l |C_l(t)|^2 = 2 \sum_l \mathbb{R} \left[\frac{-i}{\hbar} \cancel{\epsilon_{B\theta}^l} C_l(t)^* \cancel{C_l(t)} - \sum_k \left[C_l(t)^* C_k(t) d_{lk}^{ad} - (A_l - B_l) C_l(t)^* C_l(t) \right] \right] \quad (\text{E.2})$$

$$= -2 \sum_l \mathbb{R} \left[\sum_k \left[C_l(t)^* C_k(t) d_{lk}^{ad} - (A_l - B_l) C_l(t)^* C_l(t) \right] \right] \quad (\text{E.3})$$

Where:

$$A_l = \sum_{v=1}^{N_n} \sum_k \frac{\mathcal{Q}_{lk,v}(t)}{\hbar M_v} \cdot \mathbf{f}_{k,v}(t) |C_k(t)|^2 \quad (\text{E.4})$$

$$B_l = \sum_{v=1}^{N_n} \sum_k \frac{\mathcal{Q}_{lk,v}(t)}{\hbar M_v} \cdot \mathbf{f}_{l,v}(t) |C_k(t)|^2 \quad (\text{E.5})$$

The NACE term evaluates to 0 due to the anti-symmetry of the NACE giving us equation (E.7).

So far, we have proved that the norm should be conserved here for all terms apart from the quantum momentum terms i.e. Ehrenfest.

$$\frac{d}{dt} \sum_l |C_l^{QM}(t)|^2 = 2 \sum_l \Re[(A_l - B_l) C_l(t)^* C_l(t)] \quad (\text{E.6})$$

$$= 2 \left[\sum_l A_l |C_l(t)|^2 - \sum_l B_l |C_l(t)|^2 \right] \quad (\text{E.7})$$

However, $\sum_l A_l |C_l|^2 \equiv \sum_l B_l |C_l|^2$, therefore there is no change in the population and the norm should be conserved.

Appendix F

Dynamic σ Calculation

The algorithm for dynamically updating the σ parameter outlined in Gossel, 18³ is provided below.

1. Set an initial width parameter ($\sigma_v^{(I)}(t - dt)$) and a constant we will name D .
2. Calculate a cutoff distance via: $r_{cut}(t) = D\sigma_v^{(I)}(t - dt)$.
3. For each atom index, v , and replica, I , gather replicas within a cutoff distance of the current replica. Set the number of replicas within the cutoff distance to N .
4. Calculate the distance between atoms on different replicas.
5. Find the standard deviation of these distances and set the width of the gaussian, centered on atom v and replica I , to this standard deviation.
6. If the standard deviation is smaller than $\frac{D}{N} \min_I [\sigma_v^{(I)}(t - dt)]$ then set $\sigma_v^{(I)}(t) = \frac{D}{N} \min_I [\sigma_v^{(I)}(t - dt)]$.

Appendix G

Basis Transformation

We can expand the Schrödinger equation in terms of a diabatic basis, ϕ rather than an adiabatic one, ψ . These 2 expansions are given in equations (G.1) and (G.2).

$$|\Psi\rangle = \sum_n C_n |\psi_n\rangle \quad (\text{G.1})$$

$$|\Psi\rangle = \sum_l u_l |\phi_l\rangle \quad (\text{G.2})$$

It follows from this we can define a transformation matrix, U_{ln} to transform between the adiabatic and diabatic bases. This is shown in equation (G.3) where the $\overset{\leftrightarrow}{I}$ symbol represents the identity matrix. This identity only holds in the orthogonal diabatic basis ϕ and wouldn't hold for non-orthogonal bases.

$$|\psi_n\rangle = \overset{\leftrightarrow}{I} |\psi_n\rangle = \sum_l |\phi_l\rangle \langle \phi_l| \psi_n\rangle = \sum_l |\phi_l\rangle U_{ln} \quad (\text{G.3})$$

A similar relation between expansion coefficients exists

$$\sum_n C_n |\psi_n\rangle = \sum_l u_l |\phi_l\rangle \quad (\text{G.4})$$

$$\sum_n C_n \langle \psi_m | \psi_n \rangle = \sum_l u_l \langle \psi_m | \phi_l \rangle \quad (\text{G.5})$$

$$C_m = \sum_l u_l U_{lm}^* \quad (\text{G.6})$$

Finally an important property of the transformation matrix is given in equation (G.7).

$$\sum_m U_{im} U_{lm}^* = \sum_m \langle \phi_i | \psi_m \rangle \langle \psi_m | \phi_l \rangle = \langle \phi_i | \phi_l \rangle = \delta_{il} \quad (\text{G.7})$$

Equations (G.3), (G.6) and (G.7) will be used below to transform the propagation equations from the adiabatic basis to the diabatic one.

G.1 Forces

The equation for the propagation of the forces in the adiabatic basis is:

$$\begin{aligned} \mathbf{F}_v^{(I)} = & - \sum_n |C_n^{(I)}|^2 \nabla_v E_n^{(I)} - \sum_{n,m} C_m^{*(I)} C_n^{(I)} \left(E_n^{(I)} - E_m^{(I)} \right) \mathbf{d}_{v,mn}^{ad,(I)} \\ & - \sum_{m,n} |C_m^{(I)}|^2 \left(\sum_{v'}^{N_n} \frac{2}{\hbar M_{v'}} \mathcal{Q}_{v',mn}^{(I)} \cdot \mathbf{f}_{m,v'}^{(I)} \right) [\mathbf{f}_{n,v}^{(I)} - \mathbf{f}_{m,v}^{(I)}] |C_n^{(I)}|^2 \end{aligned} \quad (\text{G.8})$$

The quantum momentum part of the equation cannot be easily transformed so this will focus on the Ehrenfest part:

$$\mathbf{F}_{eh,v}^{(I)} = - \sum_n |C_n^{(I)}|^2 \nabla_v E_n^{(I)} - \sum_{n,m} C_m^{*(I)} C_n^{(I)} \left(E_n^{(I)} - E_m^{(I)} \right) \mathbf{d}_{v,mn}^{ad,(I)} \quad (\text{G.9})$$

Using equation (10) in Carof, 17⁶⁴ and the Hellman-Feynman theorem we can rewrite equation (G.9) as equation (G.10):

$$\mathbf{F}_{eh,v}^{(I)} = \sum_{m,n} C_m^{*(I)} C_n^{(I)} \langle \psi_m | \nabla_v H | \psi_n \rangle \quad (\text{G.10})$$

We can substitute the coefficients and basis functions for those in equations (G.3) and (G.6). This carried out in equation (G.15). However, I have removed the trajectory and

atom index from the terms to make the notation clearer.

$$F_{eh,v} = \sum_{m,n} C_m^* C_n \langle \psi_m | \nabla H | \psi_n \rangle \quad (\text{G.11})$$

$$= \sum_{m,n} \sum_i u_i^* U_{im} \sum_j u_j U_{jn}^* \sum_l U_{lm}^* \sum_k U_{kn} \langle \phi_l | \nabla H | \phi_k \rangle \quad (\text{G.12})$$

$$= \sum_{m,n} \sum_{i,j,k,l} u_i^* u_j U_{im} U_{lm}^* U_{jn}^* U_{kn} \langle \phi_l | \nabla H | \phi_k \rangle \quad (\text{G.13})$$

$$= \sum_{i,j,k,l} u_i^* u_j \delta_{il} \delta_{jk} \langle \phi_l | \nabla H | \phi_k \rangle \quad (\text{G.14})$$

$$= \sum_{i,j} u_i^* u_j \langle \phi_i | \nabla H | \phi_j \rangle \quad (\text{G.15})$$

However, in the code the expectation value of the gradient of the Hamiltonian ($\langle \phi_i | \nabla H | \phi_j \rangle$) isn't very easily calculable. However, the gradient of the Hamiltonian matrix elements ($\nabla \langle \phi_i | H | \phi_j \rangle$) is easily calculable via the overlap term, $\nabla H = C \nabla S_{ij}$. Therefore, using chain rule we can re-write equation (G.15) as:

$$F_{eh,v} = \sum_{i,j} u_i^* u_j \langle \phi_i | \nabla H | \phi_j \rangle \quad (\text{G.16})$$

$$= \sum_{i,j} u_i^* u_j (\nabla \langle \phi_i | H | \phi_j \rangle - \langle \nabla \phi_i | H | \phi_j \rangle - \langle \phi_i | H | \nabla \phi_j \rangle) \quad (\text{G.17})$$

$$= \sum_{i,j} u_i^* u_j \left(\nabla \langle \phi_i | H | \phi_j \rangle - \sum_l \langle \nabla \phi_i | \phi_l \rangle \langle \phi_l | H | \phi_j \rangle - \sum_l \langle \phi_i | H | \phi_l \rangle \langle \phi_l | \nabla \phi_j \rangle \right) \quad (\text{G.18})$$

$$= \sum_{i,j} u_i^* u_j \left(\nabla \langle \phi_i | H | \phi_j \rangle + \sum_l \mathbf{d}_{il} \langle \phi_l | H | \phi_j \rangle - \sum_l \mathbf{d}_{lj} \langle \phi_i | H | \phi_l \rangle \right) \quad (\text{G.19})$$

Giving the final equation for the transformed forces as:

$$\mathbf{F}_{eh,v}^{(I)} = \sum_{i,j} \mathbf{u}_i^{*(I)} \mathbf{u}_j^{(I)} \left(\nabla_v H_{ij}^{(I)} + \sum_l \mathbf{d}_{lk,v}^{(I)} H_{lj}^{(I)} - \sum_l \mathbf{d}_{lj,v}^{(I)} H_{il} \right) \quad (\text{G.20})$$

Appendix H

Adiabatic State Initialisation

By diagonalising the Hamiltonian we get the adiabatic energies (eigenvalues) for each state and transformation matrix (eigenvectors) to calculate diabatic states \mathbb{U} . We can calculate diabatic coefficients corresponding to each adiabatic state via equation (H.1) below.

$$\mathbb{U}\mathbf{C}_n = \mathbf{u}_n \quad (\text{H.1})$$

Where \mathbb{U} is the transformation matrix of size $(N_{\text{mol}}, N_{\text{mol}})$, \mathbf{C} is a complex vector of size N_{mol} containing coefficients for adiabatic state n and \mathbf{u} is a complex vector of size N_{mol} containing coefficients for diabatic state n .

Seeing as we would like to find the diabatic population corresponding to each adiabatic state we localise coefficients on each pure adiabatic state and carry out the transformation e.g: $C_i = (1+0i, 0+0i, 0+0i, \dots)$ when we want to find the diabatic coefficient corresponding to state 1 and $C_i = (0+0i, 1+0i, 0+0i, \dots)$ when we want to find the diabatic coefficient corresponding to state 2 etc.. Therefore, the column, n , of the transformation matrix, \mathbb{U} , gives the diabatic coefficients corresponding to adiabatic state, n , as shown below in equation (H.2)

$$U_{in} = u_i \quad (\text{H.2})$$

Where n is the adiabatic state index and i is the diabatic (molecular) state index.

Once we have the diabatic state corresponding to each adiabatic state, and the en-

ergy of that adiabatic state, we can find which state best fulfills the requirements of being close to the center of the system and being within $3KT$ of the ground state. In order to do this, we can loop over each adiabatic state in increasing order of energy. The center of the system is calculated and the population weighted average center of mass, \mathbf{R}_n of the diabatic coefficients corresponding to adiabatic state n is calculated as in equation (H.3).

$$\mathbf{R}_n = \sum_i |u_i|^2 \mathbf{R}_{COM,i} \quad (\text{H.3})$$

The Euclidean distance between the center of the system and $\mathbf{R}_{COM,i}$ is calculated and if this distance is below some threshold value then we initialise the surface hopping trajectory on that adiabatic state. If we do not find any states within $3KT$ of the ground state and within an acceptable radius of the center we start again this time increasing the maximum allowed distance from the center. If this maximum allowed distance is increased such that we reach another threshold distance the energy threshold is increased this time until a state is found that is close enough to the center. In this way we find an adiabatic state, which when transformed, gives a diabatic population close to center of the system and near the ground state energy.

Appendix I

Center of Mass Restraints

The surface hopping code at the time did not support electrostatic interactions. So, in order to maintain the structure from the molecular dynamics simulations, center of mass restraints were used on each molecule.

The restraint set up for 1 molecule is shown in figure I.1. Here each of the 4 coloured zig-zag shapes show which atoms are restrained. These atoms were restrained about their center of mass. This configuration of restraints was used in order to stop rotations about the long axis for each molecule as this would allow molecules to form a face-to-face stacking giving rise to unphysically high couplings. The restraint strength was chosen to be the same as in another group members study to allow for a fair comparison of results. A short MD equilibration was performed to determine whether the restraint spring constant was sufficient to hold the molecules in place well enough to prevent the very high couplings appearing in the global coupling distribution. To further validate the choice of restraint/general set up a surface hopping simulation was carried out on a layer of bulk crystal and the mobilities were compared to known values.

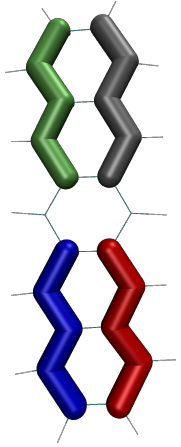


Figure I.1: The restraint set up for 1 molecule. Each coloured zig-zag shows the atoms that are restrained.

Appendix J

Active Systems

J.1 0ns and 1ns Systems

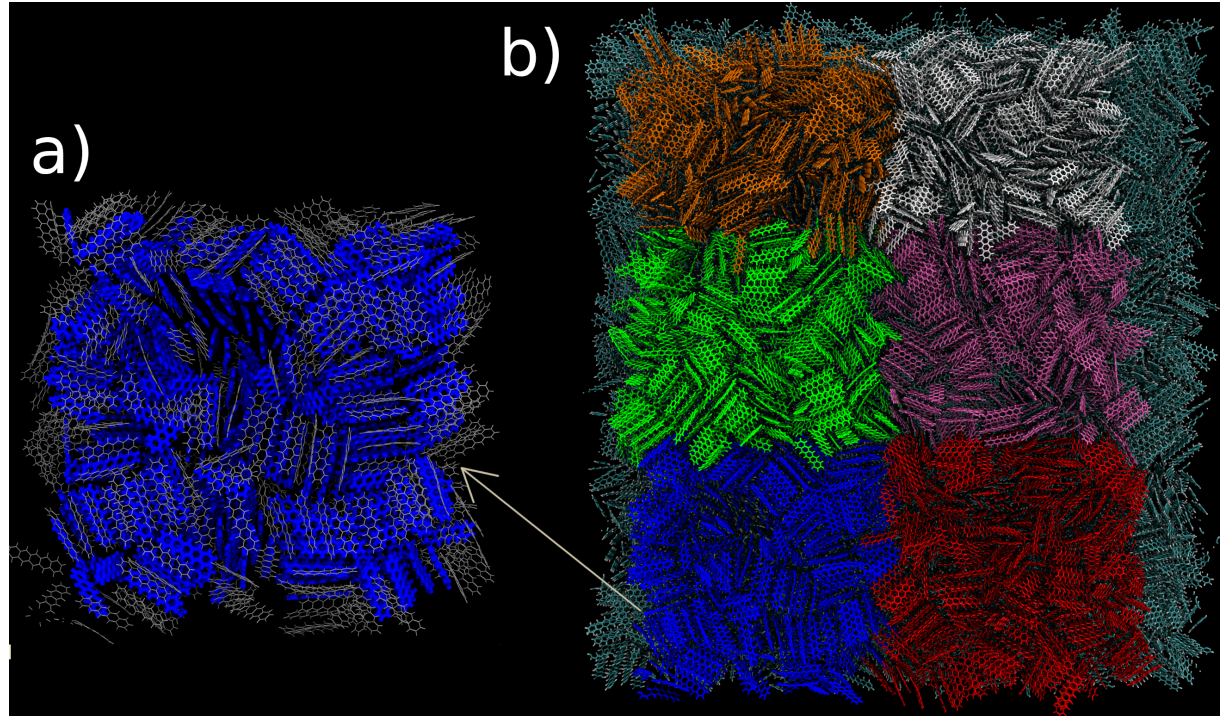


Figure J.1: Panel a) shows a system chosen to run surface hopping on, molecules in gray are fixed in place blue molecules show the active region. Panel b) shows every substructure chosen in the 0ns quenched structure.

The selection of the region for each surface hopping simulation was important in order to get a fair representation of the mobilities achievable within each structure. In the 0ns and 1ns quenched structures 6 slices were selected from the final snapshot of the structure. These were chosen to be independent clusters evenly spaced to sample

the mobility of the structure at various points. The selections are shown in figure J.1 for the 0ns quenched structure. The same process was used in the 1ns quenched structure.

In order to preserve the structure and maintain energy conservation a shell of inactive molecules was selected from the superstructure to surround the active region. The atoms within this remained fixed to their position at t=0.

J.2 100ns System

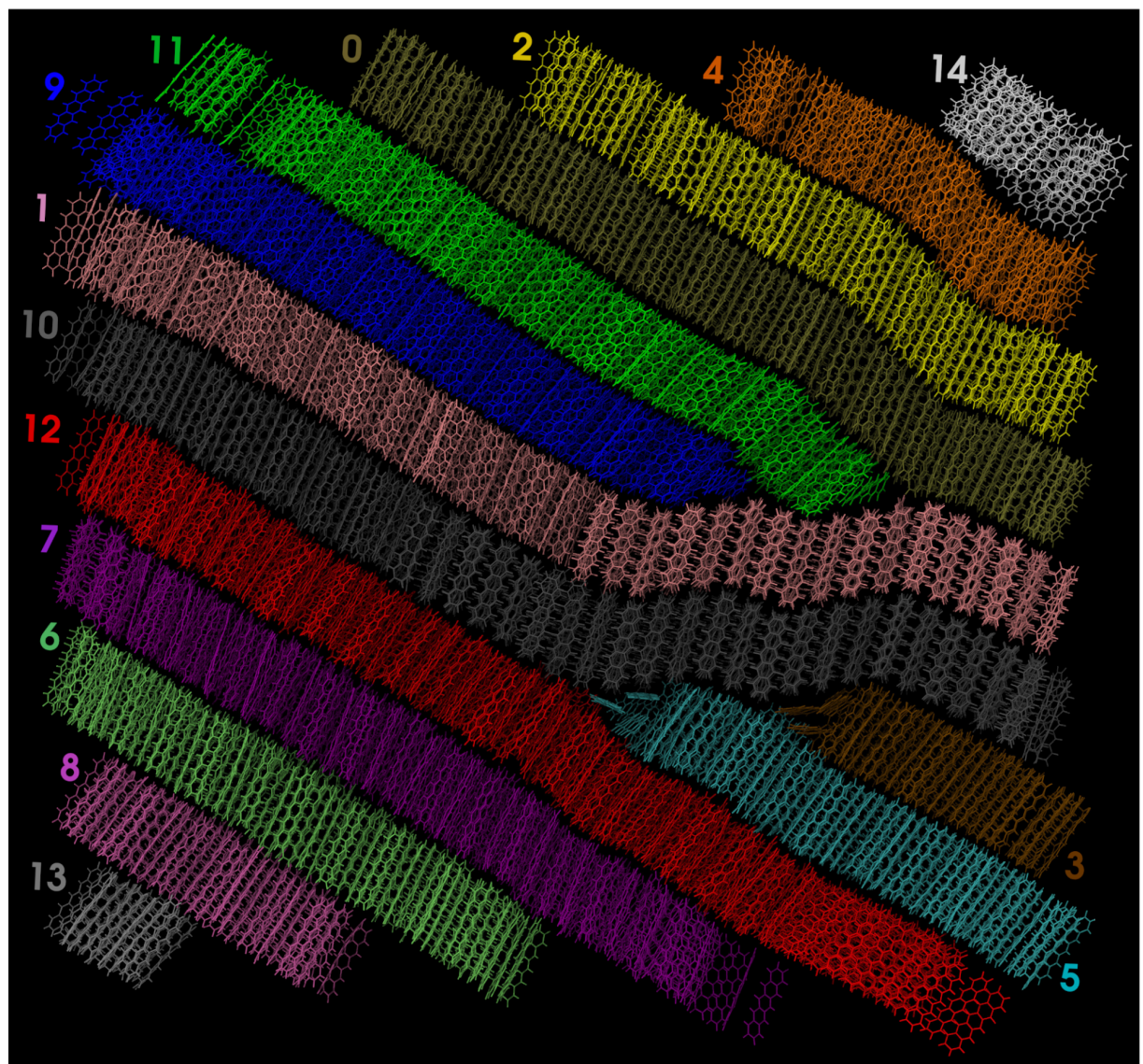


Figure J.2: The 100ns quenched structure clustered by layer. Each different colour represents a different cluster, labelled with the numbers around the edge of the structure.

The 100ns system is a much more ordered system and forms very well defined layers. This makes picking out structures on which to run surface hopping different to the 0/1ns quenched structures. The method I used was to first extend the superstructure in the z axis by $\pm 45\text{\AA}$ by repeating the periodic image and discarding molecules more than $\pm 45\text{\AA}$ from the simulation box boundaries. This was to ensure the resulting system was sufficiently large to converge mobilities. This added approximately 1 extra periodic image in the +ve and -ve z direction. A density based clustering algorithm (similar to DBSCAN¹⁰⁷) was used to isolate the layers in the full structure by clustering centers of mass. These are shown in figure J.2. In this figure clusters 6, 7 and 11 were chosen to calculate the mobility via surface hopping.

J.3 10ns System

The choice of region within the 10ns quenched structure was different from the 0/1ns and the 100ns quenched structure. Here we have some large crystal fragments forming but still very few well defined layers. In this system the mobility is expected to be much more dependant on the initial position of the charge carrier within the structure than in the 0ns and 100ns quenched structure where the structure was more uniformly disordered or ordered respectively. In order to sample a reasonable range of mobilities in this structure 4 clusters were selected shown in fig J.3. 3 of these (red, blue and purple) were selected using a similar clustering procedure as in the 100ns quenched structure. The center-right green cluster was selected as it looked like it was a fairly disordered region where multiple crystal fragments

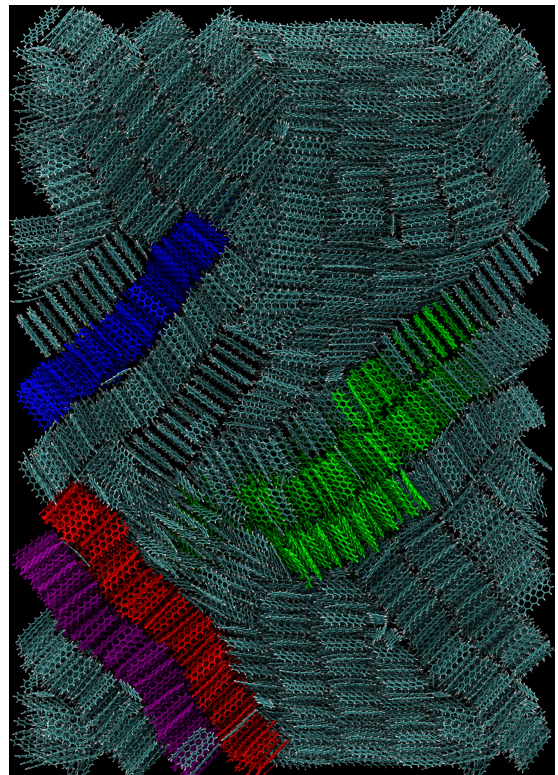


Figure J.3: The clusters chosen to run surface hopping simulations on. The coloured clusters each represent a different structure on which surface hopping was ran.

meet, which would give a lower bound on the mobility within the 10ns structure.

Appendix K

Analytic Overlap Method

Appendix L

Addition-Subtraction Forces

L.1 Real Space

The real space forces in the addition subtraction scheme are given in equation (L.1).

$$\mathbf{F}_i^\gamma = \begin{cases} \mathbf{F}_i^N(\mathbf{R}) + \sum_{j \in \gamma} (q_i^C q_j^C - q_i^N q_j^N) \mathbf{f}_{ij}(\mathbf{R}) + \sum_{j \notin \gamma} (q_i^C q_j^N - q_i^N q_j^N) \mathbf{f}_{ij}(\mathbf{R}); & i \in \gamma \\ \mathbf{F}_i^N(\mathbf{R}) - \sum_{j \in \gamma} (q_i^C q_j^N - q_i^N q_j^N) \mathbf{f}_{ij}(\mathbf{R}); & i \notin \gamma \end{cases} \quad (\text{L.1})$$

Where:

- $\mathbf{f}_{ij}(\mathbf{R}) = \frac{\hat{\mathbf{R}}_{ij}}{|\mathbf{R}_{ij}|} \left(\frac{\operatorname{erfc}(\alpha |\mathbf{R}_{ij}|)}{|\mathbf{R}_{ij}|} + \frac{2\alpha}{\sqrt{\pi}} e^{-\alpha^2 |\mathbf{R}_{ij}|^2} \right)$: the force between atoms i and j.
- $\mathbf{F}_i^N(\mathbf{R}) = q_i^N \sum_j^{N_{at}} q_j^N \mathbf{f}_{ij}(\mathbf{R})$: the total neutral force.
- q_j is the charge on atom j
- γ is the index of the charged molecule.

Once again, we first calculate the total force between all neutral molecules. The charge-charge interactions are substituted in for the neutral-neutral interactions for atoms on the charged molecule. The charge-neutral interactions are then substituted in for the neutral-neutral interactions for the charged molecule and its environment. The bonded interaction corrections are the same as these.

L.2 Reciprocal Space

The reciprocal space forces, as mentioned in the main text, cannot be decomposed with the addition-subtraction scheme.

$$\mathbf{F}_i^\gamma(\mathbf{R}) = \begin{cases} 4\pi q_i^C \sum_{\mathbf{k} \neq 0} \text{Im} [S'_\mathbf{k} E_{\mathbf{k},i}^*]; & i \in \gamma \\ 4\pi q_i^N \sum_{\mathbf{k} \neq 0} \text{Im} [S'_\mathbf{k} E_{\mathbf{k},i}^*]; & i \notin \gamma \end{cases} \quad (\text{L.2})$$

Where:

- $S'_\mathbf{k} = A_\mathbf{k} \left[\sum_j q_j^N E_{\mathbf{k},j} + \sum_{j \in \gamma} (q_j^C - q_j^N) E_{\mathbf{k},j} \right]$
- $A_\mathbf{k} = \frac{\mathbf{k}}{|\mathbf{k}|^2} e^{\frac{|\mathbf{k}|^2}{4\alpha^2}}$
- $E_{\mathbf{k},j} = e^{2\pi i \mathbf{k} \cdot \mathbf{R}_j}$

The calculation of this equation scales as $\mathcal{O}(N^3)$ where $N^3 = N_{\text{states}} N_{\text{at}} N_k$. This is because for every atom, i , in charged molecule, γ , a loop over \mathbf{k} vectors must be calculated.

Appendix M

Colophon

This is a description of the tools you used to make your thesis. It helps people make future documents, reminds you, and looks good.

(example) This document was set in the Times Roman typeface using L^AT_EX (specifically LuaTeX) and BibTeX, composed with Vim Used Archer, Kathleen etc...

Bibliography

- [1] Federica Agostini, Ali Abedi, Yasumitsu Suzuki, Seung Kyu Min, Neepa T. Maitra, and E. K. U. Gross. The exact forces on classical nuclei in non-adiabatic charge transfer. *The Journal of Chemical Physics*, 142(8):084303, February 2015.
- [2] Federica Agostini, Seung Kyu Min, Ali Abedi, and E. K. U. Gross. Quantum-Classical Nonadiabatic Dynamics: Coupled- vs Independent-Trajectory Methods. *Journal of Chemical Theory and Computation*, 12(5):2127–2143, May 2016.
- [3] Graeme H. Gossel, Federica Agostini, and Neepa T. Maitra. Coupled-Trajectory Mixed Quantum-Classical Algorithm: A Deconstruction. *Journal of Chemical Theory and Computation*, August 2018.
- [4] William Humphrey, Andrew Dalke, and Klaus Schulten. VMD – Visual Molecular Dynamics. *Journal of Molecular Graphics*, 14:33–38, 1996.
- [5] John Stone. An Efficient Library for Parallel Ray Tracing and Animation. Master’s thesis, Computer Science Department, University of Missouri-Rolla, April 1998.
- [6] C. K. Chiang, C. R. Fincher, Y. W. Park, A. J. Heeger, H. Shirakawa, E. J. Louis, S. C. Gau, and Alan G. MacDiarmid. Electrical Conductivity in Doped Polyacetylene. *Physical Review Letters*, 39(17):1098–1101, October 1977.
- [7] Hideki Shirakawa, Edwin J. Louis, Alan G. MacDiarmid, Chwan K. Chiang, and Alan J. Heeger. Synthesis of electrically conducting organic polymers: halogen derivatives of polyacetylene, $(CH)_x$. *J. Chem. Soc., Chem. Commun.*, 0(16):578–580, Jan 1977.

- [8] Bernard Kippelen and Jean-Luc Brédas. Organic photovoltaics. *Energy Environ. Sci.*, 2(3):251–261, 2009.
- [9] M. J. Małachowski and J. Żmija. Organic field-effect transistors. *Opto-Electron. Rev.*, 18(2):121–136, Jun 2010.
- [10] N. Thejo Kalyani and S. J. Dhoble. Organic light emitting diodes: Energy saving lighting technology—A review. *Renewable Sustainable Energy Rev.*, 16(5):2696–2723, Jun 2012.
- [11] Sebastian Reineke, Frank Lindner, Gregor Schwartz, Nico Seidler, Karsten Walzer, Björn Lüssem, and Karl Leo. White organic light-emitting diodes with fluorescent tube efficiency. *Nature*, 459(7244):234, May 2009.
- [12] Kazuki Kato, Toshihiko Iwasaki, and Takatoshi Tsujimura. Over 130 lm/w all-phosphorescent white oleds for next-generation lighting. *Journal of Photopolymer Science and Technology*, 28:335–340, 10 2015.
- [13] Veaceslav Coropceanu, Jérôme Cornil, Demetrio A. da Silva Filho, Yoann Olivier, Robert Silbey, and Jean-Luc Brédas. Charge Transport in Organic Semiconductors. *Chemical Reviews*, 107(4):926–952, April 2007.
- [14] Samuele Giannini, Antoine Carof, Matthew Ellis, Hui Yang, Orestis George Ziogos, Soumya Ghosh, and Jochen Blumberger. Quantum localization and delocalization of charge carriers in organic semiconducting crystals. *Nature Communications*, 10(1):3843, Aug 2019.
- [15] Alessandro Troisi. Charge transport in high mobility molecular semiconductors: classical models and new theories. *Chem. Soc. Rev.*, 40:2347–2358, 2011.
- [16] Simone Fratini, Didier Mayou, and Sergio Ciuchi. The transient localization scenario for charge transport in crystalline organic materials. *Advanced Functional Materials*, 26(14):2292–2315, 2016.

- [17] I. Yavuz. Dichotomy between the band and hopping transport in organic crystals: insights from experiments. *Physical Chemistry Chemical Physics*, 19(38):25819–25828, 2017.
- [18] Tahereh Nematiaran, Sergio Ciuchi, Xiaoyu Xie, Simone Fratini, and Alessandro Troisi. Practical computation of the charge mobility in molecular semiconductors using transient localization theory. *The Journal of Physical Chemistry C*, 123(12):6989–6997, Mar 2019.
- [19] S. Ciuchi, S. Fratini, and D. Mayou. Transient localization in crystalline organic semiconductors. *Phys. Rev. B*, 83:081202, Feb 2011.
- [20] Haobin Wang and Michael Thoss. A multilayer multiconfigurational time-dependent hartree study of vibrationally coupled electron transport using the scattering state representation. *The journal of physical chemistry. A*, 117, 03 2013.
- [21] Chr. Cattarius, G. A. Worth, H.-D. Meyer, and L. S. Cederbaum. All mode dynamics at the conical intersection of an octa-atomic molecule: Multi-configuration time-dependent Hartree (MCTDH) investigation on the butatriene cation. *The Journal of Chemical Physics*, 115(5):2088–2100, August 2001.
- [22] Uwe Manthe and Audrey Dell Hammerich. Wavepacket dynamics in five dimensions. photodissociation of methyl iodide. *Chemical Physics Letters*, 211(1):7–14, 1993.
- [23] U. Manthe, H.-D. Meyer, and L. S. Cederbaum. Multiconfigurational time-dependent hartree study of complex dynamics: Photodissociation of no₂. *The Journal of Chemical Physics*, 97(12):9062–9071, 1992.
- [24] A. Jäckle and H.-D. Meyer. Reactive scattering using the multiconfiguration time-dependent hartree approximation: General aspects and application to the collinear h+h₂→h₂+h reaction. *The Journal of Chemical Physics*, 102(14):5605–5615, 1995.
- [25] John C. Tully. Molecular dynamics with electronic transitions. *The Journal of Chemical Physics*, 93(2):1061–1071, 1990.

- [26] P. Ehrenfest. Bemerkung über die angenäherte gültigkeit der klassischen mechanik innerhalb der quantenmechanik. *Zeitschrift für Physik*, 45(7):455–457, Jul 1927.
- [27] D. F. Coker and L. Xiao. Methods for molecular dynamics with nonadiabatic transitions. *J. Chem. Phys.*, 102(1):496–510, Jan 1995.
- [28] Guangjun Nan, Xiaodi Yang, Linjun Wang, Zhigang Shuai, and Yi Zhao. Nuclear tunneling effects of charge transport in rubrene, tetracene, and pentacene. *Phys. Rev. B*, 79:115203, Mar 2009.
- [29] Sharon Hammes-Schiffer. Theoretical Perspectives on Proton-Coupled Electron Transfer Reactions. *Acc. Chem. Res.*, 34(4):273–281, Apr 2001.
- [30] Sharon Hammes-Schiffer and John C. Tully. Proton transfer in solution: Molecular dynamics with quantum transitions. *J. Chem. Phys.*, 101(6):4657–4667, Sep 1994.
- [31] My Hang V. Huynh and Thomas J. Meyer. Proton-coupled electron transfer. *Chemical Reviews*, 107(11):5004–5064, Nov 2007.
- [32] John C. Tully. Nonadiabatic Dynamics. pages 34–71.
- [33] Simone Pisana, Michele Lazzeri, Cinzia Casiraghi, Kostya S. Novoselov, A. K. Geim, Andrea C. Ferrari, and Francesco Mauri. Breakdown of the adiabatic Born–Oppenheimer approximation in graphene. *Nat. Mater.*, 6(3):198, Feb 2007.
- [34] M. Born and R. Oppenheimer. Zur Quantentheorie der Moleküle. *Ann. Phys.*, 389(20):457–484, Jan 1927.
- [35] Xiaosong Li, John C. Tully, H. Bernhard Schlegel, and Michael J. Frisch. Ab initio Ehrenfest dynamics. *J. Chem. Phys.*, 123(8):084106, Aug 2005.
- [36] Kenichiro Saita and Dmitrii V. Shalashilin. On-the-fly ab initio molecular dynamics with multiconfigurational Ehrenfest method. *J. Chem. Phys.*, 137(22):22A506, Dec 2012.
- [37] Daniela Kohen, Frank H. Stillinger, and John C. Tully. Model studies of nonadiabatic dynamics. *J. Chem. Phys.*, 109(12):4713–4725, Sep 1998.

- [38] John C. Tully. Perspective: Nonadiabatic dynamics theory. *The Journal of Chemical Physics*, 137(22):22A301, December 2012.
- [39] Priya V. Parandekar and John C. Tully. Detailed Balance in Ehrenfest Mixed Quantum-Classical Dynamics. *Journal of Chemical Theory and Computation*, 2(2):229–235, March 2006.
- [40] Ali Abedi, Neepa T. Maitra, and E. K. U. Gross. Exact Factorization of the Time-Dependent Electron-Nuclear Wave Function. *Physical Review Letters*, 105(12), September 2010.
- [41] Federica Agostini, Seung Kyu Min, and E. K. U. Gross. Semiclassical analysis of the electron-nuclear coupling in electronic non-adiabatic processes. *Annalen der Physik*, 527(9-10):546–555, October 2015.
- [42] Federica Agostini, Ali Abedi, Yasumitsu Suzuki, and E.K.U. Gross. Mixed quantum-classical dynamics on the exact time-dependent potential energy surface: a fresh look at non-adiabatic processes. *Molecular Physics*, 111(22-23):3625–3640, December 2013.
- [43] Ali Abedi, Federica Agostini, Yasumitsu Suzuki, and E. K. U. Gross. Dynamical Steps that Bridge Piecewise Adiabatic Shapes in the Exact Time-Dependent Potential Energy Surface. *Physical Review Letters*, 110(26), June 2013.
- [44] Seung Kyu Min, Ali Abedi, Kwang S. Kim, and E. K. U. Gross. Is the Molecular Berry Phase an Artifact of the Born-Oppenheimer Approximation? *Phys. Rev. Lett.*, 113(26):263004, Dec 2014.
- [45] Todd J. Martínez*. Insights for Light-Driven Molecular Devices from Ab Initio Multiple Spawning Excited-State Dynamics of Organic and Biological Chromophores. American Chemical Society, Oct 2005.
- [46] Farnaz A. Shakib and Pengfei Huo. Ring Polymer Surface Hopping: Incorporating Nuclear Quantum Effects into Nonadiabatic Molecular Dynamics Simulations. *J. Phys. Chem. Lett.*, 8(13):3073–3080, Jul 2017.

- [47] Basile F. E. Curchod, Ivano Tavernelli, and Ursula Rothlisberger. Trajectory-based solution of the nonadiabatic quantum dynamics equations: an on-the-fly approach for molecular dynamics simulations. *PCCP*, 13(8):3231–3236, Feb 2011.
- [48] Ivano Tavernelli. Ab initio–driven trajectory-based nuclear quantum dynamics in phase space. *Phys. Rev. A*, 87(4):042501, Apr 2013.
- [49] Arne Scherrer, Federica Agostini, Daniel Sebastiani, E. K. U. Gross, and Rodolphe Vuilleumier. Nuclear velocity perturbation theory for vibrational circular dichroism: An approach based on the exact factorization of the electron-nuclear wave function. *J. Chem. Phys.*, 143(7):074106, Aug 2015.
- [50] Seung Kyu Min, Federica Agostini, Ivano Tavernelli, and E. K. U. Gross. Ab Initio Nonadiabatic Dynamics with Coupled Trajectories: A Rigorous Approach to Quantum (De)Coherence. *The Journal of Physical Chemistry Letters*, 8(13):3048–3055, July 2017.
- [51] John C. Tully. Molecular dynamics with electronic transitions. *The Journal of Chemical Physics*, 93(2):1061–1071, July 1990.
- [52] Fruzsina Gajdos, Siim Valner, Felix Hoffmann, Jacob Spencer, Marian Breuer, Adam Kubas, Michel Dupuis, and Jochen Blumberger. Ultrafast Estimation of Electronic Couplings for Electron Transfer between -Conjugated Organic Molecules. *Journal of Chemical Theory and Computation*, 10(10):4653–4660, October 2014.
- [53] J. VandeVondele, J; Hutter. Gaussian basis sets for accurate calculations on molecular systems in gas and condensed phases. *The Journal of Chemical Physics*, 127(11).
- [54] J. Spencer, F. Gajdos, and J. Blumberger. FOB-SH: Fragment orbital-based surface hopping for charge carrier transport in organic and biological molecules and materials. *The Journal of Chemical Physics*, 145(6):064102, August 2016.
- [55] Steven L. Fiedler and Jussi Eloranta. Nonadiabatic dynamics by mean-field and surface-hopping approaches: energy conservation considerations. *Molecular Physics*, 108(11):1471–1479, 2010.

- [56] Joseph E. Subotnik. Augmented ehrenfest dynamics yields a rate for surface hopping. *The Journal of Chemical Physics*, 132(13):134112, 2010.
- [57] K.E. Atkinson. *An Introduction to Numerical Analysis*. Wiley, 1989.
- [58] R.B. Leighton Richard P. Feynman. *The Feynman Lectures on Physics*, Vol 3. Addison–Wesley, 1998.
- [59] James Kirkpatrick. An approximate method for calculating transfer integrals based on the zindo hamiltonian. *International Journal of Quantum Chemistry*, 108(1):51–56, 2008.
- [60] Harald Oberhofer and Jochen Blumberger. Revisiting electronic couplings and incoherent hopping models for electron transport in crystalline c60 at ambient temperatures. *Phys. Chem. Chem. Phys.*, 14:13846–13852, 2012.
- [61] Alessandro Troisi and Giorgio Orlandi. Hole migration in dna: a theoretical analysis of the role of structural fluctuations. *The Journal of Physical Chemistry B*, 106(8):2093–2101, Feb 2002.
- [62] Adam Kubas, Felix Hoffmann, Alexander Heck, Harald Oberhofer, Marcus Elstner, and Jochen Blumberger. Electronic couplings for molecular charge transfer: Benchmarking cdft, fodft, and fodftb against high-level ab initio calculations. *The Journal of Chemical Physics*, 140(10):104105, 2014.
- [63] Adam Kubas, Fruzsina Gajdos, Alexander Heck, Harald Oberhofer, Marcus Elstner, and Jochen Blumberger. Electronic couplings for molecular charge transfer: benchmarking cdft, fodft and fodftb against high-level ab initio calculations. ii. *Phys. Chem. Chem. Phys.*, 17:14342–14354, 2015.
- [64] Antoine Carof, Samuele Giannini, and Jochen Blumberger. Detailed balance, internal consistency, and energy conservation in fragment orbital-based surface hopping. *The Journal of Chemical Physics*, 147(21):214113, December 2017.

- [65] Antoine Carof, Samuele Giannini, and Jochen Blumberger. Detailed balance, internal consistency, and energy conservation in fragment orbital-based surface hopping. *The Journal of Chemical Physics*, 147(21):214113, 2017.
- [66] Soumya Ghosh, Samuele Giannini, Kevin Lively, and Jochen Blumberger. Nonadiabatic dynamics with quantum nuclei: simulating charge transfer with ring polymer surface hopping. *Faraday Discuss.*, 221:501–525, 2020.
- [67] Antoine Carof, Samuele Giannini, and Jochen Blumberger. How to calculate charge mobility in molecular materials from surface hopping non-adiabatic molecular dynamics – beyond the hopping/band paradigm. *Phys. Chem. Chem. Phys.*, 21:26368–26386, 2019.
- [68] J. Spencer, F. Gajdos, and J. Blumberger. Fob-sh: Fragment orbital-based surface hopping for charge carrier transport in organic and biological molecules and materials. *The Journal of Chemical Physics*, 145(6):064102, 2016.
- [69] Jacob Spencer, Laura Scalfi, Antoine Carof, and Jochen Blumberger. Confronting surface hopping molecular dynamics with marcus theory for a molecular donor–acceptor system. *Faraday Discuss.*, 195:215–236, 2016.
- [70] Samuele Giannini, Orestis George Ziogos, Antoine Carof, Matthew Ellis, and Jochen Blumberger. Flickering polarons extending over ten nanometres mediate charge transport in high-mobility organic crystals. *Advanced Theory and Simulations*, 3(9):2000093, 2020.
- [71] Samuele Giannini, Antoine Carof, and Jochen Blumberger. Crossover from hopping to band-like charge transport in an organic semiconductor model: Atomistic nonadiabatic molecular dynamics simulation. *The Journal of Physical Chemistry Letters*, 9(11):3116–3123, Jun 2018.
- [72] Orestis George Ziogos, Samuele Giannini, Matthew Ellis, and Jochen Blumberger. Identifying high-mobility tetracene derivatives using a non-adiabatic molecular dynamics approach. *J. Mater. Chem. C*, 8:1054–1064, 2020.

- [73] Fruzsina Gajdos, Siim Valner, Felix Hoffmann, Jacob Spencer, Marian Breuer, Adam Kubas, Michel Dupuis, and Jochen Blumberger. Ultrafast estimation of electronic couplings for electron transfer between π -conjugated organic molecules. *Journal of Chemical Theory and Computation*, 10(10):4653–4660, Oct 2014.
- [74] Biswajit Ray, Aditya G. Baradwaj, Bryan W. Boudouris, and Muhammad A. Alam. Defect characterization in organic semiconductors by forward bias capacitance–voltage (fb-cv) analysis. *The Journal of Physical Chemistry C*, 118(31):17461–17466, Aug 2014.
- [75] W. S. Hu, Y. T. Tao, Y. J. Hsu, D. H. Wei, and Y. S. Wu. Molecular orientation of evaporated pentacene films on gold: alignment effect of self-assembled monolayer. *Langmuir*, 21(6):2260–2266, Mar 2005.
- [76] Tatsuo Hasegawa and Jun Takeya. Organic field-effect transistors using single crystals. *Science and Technology of Advanced Materials*, 10(2):024314, 2009.
- [77] John E. Anthony, James S. Brooks, David L. Eaton, and Sean R. Parkin. Functionalized pentacene: improved electronic properties from control of solid-state order. *Journal of the American Chemical Society*, 123(38):9482–9483, Sep 2001.
- [78] John E. Anthony, David L. Eaton, and Sean R. Parkin. A road map to stable, soluble, easily crystallized pentacene derivatives. *Organic Letters*, 4(1):15–18, Jan 2002.
- [79] A. D’Angelo, B. Edgar, A. P. Hurt, and M. D. Antonijević. Physico-chemical characterisation of three-component co-amorphous systems generated by a melt-quench method. *Journal of Thermal Analysis and Calorimetry*, 134(1):381–390, Oct 2018.
- [80] Wanderlā L. Scopel, Antônio J. R. da Silva, and A. Fazzio. Amorphous hfo_2 and $\text{hf}_{1-x}\text{si}_x\text{O}$ via a melt-and-quench scheme using ab initio molecular dynamics. *Phys. Rev. B*, 77:172101, May 2008.
- [81] Seth S. Berbano, Inseok Seo, Christian M. Bischoff, Katherine E. Schuller, and Steve W. Martin. Formation and structure of $\text{na}_2\text{s}+\text{p}_2\text{s}_5$ amorphous materials

- prepared by melt-quenching and mechanical milling. *Journal of Non-Crystalline Solids*, 358(1):93 – 98, 2012.
- [82] Pranav Karmwar, Kirsten Graeser, Keith C. Gordon, Clare J. Strachan, and Thomas Rades. Investigation of properties and recrystallisation behaviour of amorphous indomethacin samples prepared by different methods. *International Journal of Pharmaceutics*, 417(1):94 – 100, 2011. Advanced characterization techniques.
- [83] Min-Jin Ko, Joel Plawsky, and Meyer Birnboim. Fabrication of cds/ag hybrid quantum dot composites using a melt/quench method. *Journal of Non-Crystalline Solids*, 203:211 – 216, 1996. Optical and Electrical Propertias of Glasses.
- [84] Steve Plimpton. Fast parallel algorithms for short-range molecular dynamics. *Journal of Computational Physics*, 117(1):1 – 19, 1995.
- [85] Steve Plimpton. Lammps software. <http://lammps.sandia.gov>, 1995. [Online; accessed 21-Jan-2021].
- [86] Steve Plimpton, Roy Pollock, and Mark Stevens. Particle-mesh ewald and rRESPA for parallel molecular dynamics simulations. In In Proceedings of the Eighth SIAM Conference on Parallel Processing for Scientific Computing, 1997.
- [87] Christopher I. Bayly, Piotr Cieplak, C, and Peter A. Kollman. A well-behaved electrostatic potential based method using charge restraints for deriving atomic charges: the resp model. *The Journal of Physical Chemistry*, 97(40):10269–10280, Oct 1993.
- [88] M. J. Frisch, G. W. Trucks, H. B. Schlegel, G. E. Scuseria, M. A. Robb, J. R. Cheeseman, G. Scalmani, V. Barone, G. A. Petersson, H. Nakatsuji, X. Li, M. Caricato, A. V. Marenich, J. Bloino, B. G. Janesko, R. Gomperts, B. Mennucci, H. P. Hratchian, J. V. Ortiz, A. F. Izmaylov, J. L. Sonnenberg, D. Williams-Young, F. Ding, F. Lipparini, F. Egidi, J. Goings, B. Peng, A. Petrone, T. Henderson, D. Ranasinghe, V. G. Zakrzewski, J. Gao, N. Rega, G. Zheng, W. Liang, M. Hada, M. Ehara, K. Toyota, R. Fukuda, J. Hasegawa, M. Ishida, T. Nakajima, Y. Honda,

- O. Kitao, H. Nakai, T. Vreven, K. Throssell, J. A. Montgomery, Jr., J. E. Peralta, F. Ogliaro, M. J. Bearpark, J. J. Heyd, E. N. Brothers, K. N. Kudin, V. N. Staroverov, T. A. Keith, R. Kobayashi, J. Normand, K. Raghavachari, A. P. Rendell, J. C. Burant, S. S. Iyengar, J. Tomasi, M. Cossi, J. M. Millam, M. Klene, C. Adamo, R. Cammi, J. W. Ochterski, R. L. Martin, K. Morokuma, O. Farkas, J. B. Foresman, and D. J. Fox. Gaussian[®]16 Revision C.01, 2016. Gaussian Inc. Wallingford CT.
- [89] Junmei Wang, Romain M. Wolf, James W. Caldwell, Peter A. Kollman, and David A. Case. Development and testing of a general amber force field. *Journal of Computational Chemistry*, 25(9):1157–1174, 2004.
- [90] Makoto Yoneya, Masahiro Kawasaki, and Masahiko Ando. Molecular dynamics simulations of pentacene thin films: The effect of surface on polymorph selection. *J. Mater. Chem.*, 20:10397–10402, 2010.
- [91] Makoto Yoneya, Masahiro Kawasaki, and Masahiko Ando. Are pentacene monolayer and thin-film polymorphs really substrate-induced? a molecular dynamics simulation study. *The Journal of Physical Chemistry C*, 116(1):791–795, Jan 2012.
- [92] Makoto Yoneya. Simulation of crystallization of pentacene and its derivatives from solution. *The Journal of Physical Chemistry C*, Jan 2021.
- [93] Ryan A. Miller, Amanda Larson, and Karsten Pohl. Novel surface diffusion characteristics for a robust pentacene derivative on au(111) surfaces. *Chemical Physics Letters*, 678:28 – 34, 2017.
- [94] Dong Wang, Ling Tang, Mengqiu Long, and Zhigang Shuai. Anisotropic thermal transport in organic molecular crystals from nonequilibrium molecular dynamics simulations. *The Journal of Physical Chemistry C*, 115(13):5940–5946, Apr 2011.
- [95] Florian Steiner, Carl Poelking, Dorota Niedzialek, Denis Andrienko, and Jenny Nelson. Influence of orientation mismatch on charge transport across grain boundaries in tri-isopropylsilyl ethynyl (tips) pentacene thin films. *Phys. Chem. Chem. Phys.*, 19:10854–10862, 2017.

- [96] Ida Bagus Hendra Prastiawan, Jingxiang Xu, Yusuke Ootani, Yuji Higuchi, Nobuki Ozawa, Shingo Maruyama, Yuji Matsumoto, and Momoji Kubo. Molecular interactions between pentacene and imidazolium ionic liquids: A molecular dynamics study. *Chemistry Letters*, 47(9):1154–1157, 2018.
- [97] EPA DSSTox. Epa dsstox. <https://comptox.epa.gov/dashboard/DTXSID7059648>, 2021. [Online; accessed 25-Jan-2021].
- [98] Stefan Schiefer, Martin Huth, Alexander Dobrinevski, and Bert Nickel. Determination of the crystal structure of substrate-induced pentacene polymorphs in fiber structured thin films. *Journal of the American Chemical Society*, 129(34):10316–10317, Aug 2007.
- [99] Thorsten Vehoff, Yeon Sook Chung, Karen Johnston, Alessandro Troisi, Do Y. Yoon, and Denis Andrienko. Charge transport in self-assembled semiconducting organic layers: Role of dynamic and static disorder. *The Journal of Physical Chemistry C*, 114(23):10592–10597, Jun 2010.
- [100] Wei-Qiao Deng and William A. Goddard. Predictions of hole mobilities in oligoacene organic semiconductors from quantum mechanical calculations. *The Journal of Physical Chemistry B*, 108(25):8614–8621, Jun 2004.
- [101] Joe J. Kwiatkowski, Jarvist M. Frost, and Jenny Nelson. The effect of morphology on electron field-effect mobility in disordered c₆₀ thin films. *Nano Letters*, 9(3):1085–1090, Mar 2009.
- [102] Stavros Athanasopoulos, James Kirkpatrick, Diego Martínez, Jarvist M. Frost, Clare M. Foden, Alison B. Walker, and Jenny Nelson. Predictive study of charge transport in disordered semiconducting polymers. *Nano Letters*, 7(6):1785–1788, Jun 2007.
- [103] Thorsten Vehoff, Björn Baumeier, Alessandro Troisi, and Denis Andrienko. Charge transport in organic crystals: Role of disorder and topological connectivity. *Journal of the American Chemical Society*, 132(33):11702–11708, Aug 2010.

- [104] Pascal Kordt and Denis Andrienko. Modeling of spatially correlated energetic disorder in organic semiconductors. *Journal of Chemical Theory and Computation*, 12(1):36–40, Jan 2016.
- [105] Yuan Zhang, Ling-Kun Meng, Jin Hu, Rui-Ke Zou, Chao Tang, Gong Li, Yan Ding, Hai-Tong Cai, Zhi-Yao Yang, and Wei Huang. Theoretical exploration of carrier dynamics in amorphous pyrene–fluorene derivative organic semiconductors. *ACS Omega*, 4(9):14124–14132, Aug 2019.
- [106] Orestis George Ziogos, Samuele Giannini, Matthew Ellis, and Jochen Blumberger. Identifying high-mobility tetracene derivatives using a non-adiabatic molecular dynamics approach. *J. Mater. Chem. C*, 8:1054–1064, 2020.
- [107] Martin Ester, Hans-Peter Kriegel, Jörg Sander, and Xiaowei Xu. A density-based algorithm for discovering clusters in large spatial databases with noise. pages 226–231. AAAI Press, 1996.
- [108] Nicolas G. Martinelli, Matteo Savini, Luca Muccioli, Yoann Olivier, Frédéric Castet, Claudio Zannoni, David Beljonne, and Jérôme Cornil. Modeling polymer dielectric/pentacene interfaces: On the role of electrostatic energy disorder on charge carrier mobility. *Advanced Functional Materials*, 19(20):3254–3261, 2009.
- [109] P. P. Ewald. Die berechnung optischer und elektrostatischer gitterpotentiale. *Annalen der Physik*, 369(3):253–287, 1921.
- [110] Abdulnour Y. Toukmaji and John A. Board. Ewald summation techniques in perspective: a survey. *Computer Physics Communications*, 95(2):73–92, 1996.
- [111] D. Wolf, P. Keblinski, S. R. Phillpot, and J. Eggebrecht. Exact method for the simulation of coulombic systems by spherically truncated, pairwise $r-1$ summation. *The Journal of Chemical Physics*, 110(17):8254–8282, 1999.
- [112] Dirk Zahn, Bernd Schilling, and Stefan M. Kast. Enhancement of the wolf damped coulomb potential: static, dynamic, and dielectric properties of liquid water from

- molecular simulation. *The Journal of Physical Chemistry B*, 106(41):10725–10732, Oct 2002.
- [113] Christopher J. Fennell and J. Daniel Gezelter. Is the ewald summation still necessary? pairwise alternatives to the accepted standard for long-range electrostatics. *The Journal of Chemical Physics*, 124(23):234104, 2006.
- [114] Colin R. Groom, Ian J. Bruno, Matthew P. Lightfoot, and Suzanna C. Ward. The Cambridge Structural Database. *Acta Crystallographica Section B*, 72(2):171–179, Apr 2016.